VORTEX BEHAVIORS OF CRANKED ARROW WING CONFIGURATIONS WITH DIFFERENT WING PLANFORMS

Kentaro HIRAI*, Dong-Youn KWAK** and Kenichi RINOIE*

* Department of Aeronautics and Astronautics,

University of Tokyo, Tokyo, 113-8656, JAPAN

** Japan Aerospace Exploration Agency, Tokyo, 181-0015, JAPAN

Abstract

Low speed wind tunnel measurements were done to investigate vortex behaviors and static roll characteristics of cranked arrow wing configurations for the supersonic transport with different wing planforms. Static rolling moment measurements, flow visualization studies by oil-flow and smoke were made at some Reynolds numbers. Three parameters were focused in this paper: outboard wing sweepback angles, inboard wing sweepback angles, and inboard / outboard wing kink locations. The inboard vortex behaviors are strongly influenced by the differences of outboard wing sweepback angles and thus the different rolling moment characteristics such as a hysteresis and abrupt changes in the rolling moment were observed. It was confirmed from the flow visualization analysis that the rolling moment hysteresis is caused by the different chordwise position of inboard vortex breakdown when the wing is rotated in the clockwise and counter-clockwise directions. Interaction and merge between the inboard and outboard vortices depend on the relative magnitudes of them, which affects hysteresis characteristics for the static rolling moment and vortex breakdown.

Nomenclature

b wing local span length, m

b_{max} wing maximum span length, m

b_{kink} wing kink span length, m

C_{mac} wing mean aerodynamic chord, m

C_r wing root chord at model centre-line, m

C_{rol} rolling moment coefficient non-dimensionalized using b_{max} measured about body axis x

Re Reynolds number based on mean aerodynamic chord

U_∞ free stream velocity, m/s

x chordwise coordinate measured from apex of delta wing at model centre-line, m

y spanwise coordinate orthogonal to x, fixed to the body and measured from model centre-line, m

z coordinate orthogonal to x and y measured from model centre-line, m

ϕ roll angle, degree (clockwise direction is positive when seen from downstream of the model)

θ incidence angle, degree

Λ_{in} sweepback angle at leading edge of inboard wing, degree

Λ_{out} sweepback angle at leading edge of outboard wing, degree

1 Introduction

A cranked arrow wing configuration with highly swept leading edges and low aspect ratio is one of the favorable main wing configurations of the

next generation supersonic transport (SST) [1]. At take-off and landing, the SST with a cranked arrow wing has to fly at high angles of attack (high alpha) to compensate for relatively poor aerodynamic characteristics. At high alpha flight conditions, stable leading edge separation vortices are formed on the wing and they generate the vortex lift. However, the behaviors of the leading edge separation vortices formed on the cranked arrow wing are very complicated, because two pairs of vortices are formed on the inboard and outboard wing leading edges and furthermore, because they interact with each other [2, 3]. Breakdown of these vortices over the wing also plays an important role in determining the wing characteristics. It is noted that these vortex behaviors strongly depend on the wing configurations.

When the wing is rolled statically, the effective sweepback angle on the windward wing is different from that of the leeward wing [4]. This asymmetry induces the asymmetric formation of the leading-edge vortices and the wing exhibits complex aerodynamic behaviors. Therefore, static rolling moment characteristics are one of the important factors for the aerodynamic design of delta wing aircrafts [5].

To investigate the static rolling moment characteristics of the cranked arrow wing configuration, the present authors conducted low speed wind tunnel tests [6]. Drastic changes of rolling moments from a stable to an unstable state were observed at an incidence angle of 20 degrees. It was indicated that the asymmetry of the chordwise locations of inboard vortex breakdown on the windward and leeward wings produced this drastic change.

Experimental studies using a particle image velocimetry (PIV) were made in [7] to discuss the effect of leading-edge flap deflections on the static roll characteristics of the cranked arrow SST configuration. Results indicated abrupt change and hysteresis (i.e. different rolling moments were measured when the model was rolled in the clockwise direction and when it rolled in the counter-clockwise direction) of rolling moments were observed when the outboard leading-edge flaps were deflected. It was indicated in [7] that chordwise position of the vortex breakdown on the inboard wing is

different when the wing is rotated in the clockwise and counterclockwise directions. This difference of vortex breakdown position caused the observed rolling moment hysteresis for the wing with outboard flap deflections. Based on the results in [2] and [8], reference [7] discussed that the distance between inboard and outboard vortices formed on the cranked arrow wing affects the vortex breakdown characteristics. The outboard flap deflection causes the movement of outboard vortex location which affected the inboard and outboard vortex interactions and consequently different vortex breakdown position.

It is expected that the different vortex interaction, i.e. inboard and outboard vortices are located close or away, is caused not only by use of the leading-edge flap but by the different wing planforms. Therefore, in this paper, low speed wind tunnel tests were made for cranked arrow wings with different wing planforms to understand vortex interaction behaviors between the inboard and outboard vortices formed on the wing. Following three parameters are focused on here: 1) Outboard wing sweepback angles, 2) Inboard wing sweepback angles, 3) Inboard / outboard wing kink locations. All the three parameters have been thought to affect the location of outboard and inboard vortices and hence the vortex interactions.

Experiments were conducted in a 2.0m x 2.0m circuit and a 0.6m x 0.6m blow-down low speed wind tunnels. The Reynolds number based on the mean aerodynamic chord was 6.2 x 10^4, 2.9 x 10^5, 4.3 x 10^5, 8.6 x 10^5 and 1.1 x 10^6. Force measurements and visualization tests were conducted to investigate in detail the vortex behaviors of cranked arrow wing configurations with different wing planforms.

In summary, the purpose of this study is to discuss the effect of different parameters of cranked arrow wing planforms on the static roll characteristics and to clarify the complex and non-linear behavior of the leading-edge separation vortices formed on the wing. In this paper, the effect of outboard wing sweepback angles are discussed in section two and those of inboard wing sweepback angles and inboard / outboard wing kink locations are discussed in section three.

2 Effect of Different Outboard Wing Sweep-back Angles

2.1 Experimental Details

Figure 1 shows details of the three flat plate cranked arrow wing models with different outboard sweepback angles. Although the inboard leading edge sweepback angle for each of them is 66°, the outboard leading edge sweepback angles are 30° (Type A), 42° (Type B) and 54° (Type C). The wing area for them is equally 0.292m^2, the aspect ratio is 0.242 and its thickness is 0.01m. The upper and lower surfaces of all edges are beveled.

The experiments were made in a 2m x 2m circuit type low-speed wind tunnel at the Japan Aerospace Exploration Agency. Figure 2 is a picture of the low-speed wind tunnel. Tests were mainly made at a tunnel speed of U_∞=30m/s. The Reynolds number based on the mean aerodynamic chord (C_{mac}=0.459m) was Re=8.6x10^5. To investigate the effect of Reynolds number, tests at U_∞=40m/s (Re=1.1x10^6) and U_∞=15m/s (Re=4.3x10^5) were also conducted. The incidence angle θ was in a range from 12° to 30° (this angle is equal to the angle of attack when the roll angle φ=0°). Rolling moment was measured using a six-component balance. The model was attached to the balance with a sting and can be rotated around its center axis along with the balance. The rolling moment is the roll component around the model center axis (Fig. 3). The rolling moment coefficient C_{roll} has been obtained by rolling the model at 2.5° increments from φ=-30° to +30° and by rolling back from φ=+30° to -30° which completes one measurement cycle. Additional C_{roll} measurements were made for Type C, by rolling the model at 1.0° increments from φ=-7° to +7°.

Smoke flow visualization tests were conducted to observe chordwise position of the vortex breakdown for the inboard vortex formed on the left wing in the 0.6m x 0.6m blow-down low speed wind tunnel at the University of Tokyo. The models used in these tests are similar to the original models however they are 1/5 scale of the original models. Tests were conducted at a tunnel speed of U_∞=10m/s. The Reynolds number based on the mean aerodynamic chord (C_{mac}=0.092m) was Re=6.2x10^4. Smoke made of Ondina oil was used to visualize the flow. The breakdown positions were determined with the aid of smoke flow visualization by observing the light sheet located at different chordwise positions normal to the x axis. Since the vortex breakdown position is not steady and exhibits fluctuations along the axis of the vortices [9], positions where the smoke free region near the vortex core is clearly visible and where this region is not visible at all are detected (Fig. 4). Chordwise position of the vortex breakdown was determined as a mid point of these two positions. The measured incidence angle θ was 20° and 26°. The chordwise position of the vortex breakdown has been obtained by rolling the model at 2.5° increments from φ=-30° to +30° and by rolling back from φ=+30° to -30° which completes one measurement cycle.

Furthermore, to investigate the vortex behaviors and the interaction between the inboard and outboard leading edge separation vortices, other visualization studies were conducted using the original models at the aforementioned 2m x 2m low-speed wind tunnel. Smoke made of Dioctyl sebacate oil was used to visualize the flow in these tests. The laser light sheet used to illuminate the flow was normal to the x axis. The smoke visualization movie on the right wing was recorded from downstream of the model by a VCR. Visualization images captured from the movies were obtained and processed to understand the vortex behaviors. This smoke visualization tests were conducted at U_∞=10m/s (Re=2.9x10^5) to improve the smoke density inside the flow at the same 2m x 2m wind tunnel. The incidence angle θ was 20°. The visualization movie has been obtained by rolling the model at basically 10° increments from φ=-30° to +30°. In addition, visualization tests at different rotation directions (clockwise and counter-clockwise) were conducted at the same roll angle ranges where the hysteresis has been observed in the force measurements. Nondimensional position ratios for the distance from the apex to the position of the light sheet was obtained by dividing with the root chord

length; x/Cr=0.5, 0.7, 0.8, 0.9, 1.0 (last one only for Type C). In addition, the force measurements were conducted, separately from the visualization tests, to investigate the relationships between hysteresis of C_{roll} and the vortex breakdown.

Oil flow visualization tests at U_∞=30m/s were also made to describe the surface flow pattern.

2.2 Results and Discussion

2.2.1 Overall Roll Characteristics

Figure 5 shows the results of C_{roll} versus ϕ at different θ for the different outboard sweepback angle models at Re=8.6 x 10^5. This figure indicates a linear restoring (stable) rolling moment is acting until θ=16° for all the three models. Nonlinear rolling moment characteristics are seen at θ higher than 18°. Abrupt change and rolling moment hysteresis are seen between θ=20° and 28°, i.e. different rolling moments were measured when the model was rolled in the clockwise direction (from ϕ=-30° to +30°) and when rolled in the counter-clockwise direction (from ϕ=+30° to -30°). Similar static rolling moment hysteresis has been observed for the 65° and 80° delta wings [10, 11] and for the cranked arrow wing model with outboard leading-edge flap deflection [7]. Comparing the results of the three models at the same incidence angle θ=20°, the range of the roll angle ϕ where hysteresis is observed becomes narrower when the outboard sweepback angle becomes larger (from Type A to Type C). This holds true at other incidence angles. Abrupt change of the rolling moment is observed when the hysteresis is recorded.

In Fig. 5, the hysteresis is observed only when ϕ<0 near ϕ=0° for Type C at θ=20° and 22°. Figure 6 shows results of the Type C model at the incidence angle θ=20° measured by rolling the model at 1° increment from ϕ=-7° to +7°. Although the hysteresis was not observed in the positive roll angle measured at 2.5° increments in Fig. 5, hysteresis is seen both in the positive and negative roll angle in this figure. It suggests that the roll angle range of hysteresis is very narrow in this case, and the hysteresis

was not detected in Fig. 5 because of a coarse increment of measured roll angle

2.2.2 Effects of Reynolds Number on the Static Roll Characteristics

Figure 7 shows the results of C_{roll} versus ϕ for different Reynolds numbers at the incidence angle θ=20°. Although the range of the roll angle ϕ, where hysteresis is observed, becomes wider for most of the case as Reynolds number increases, overall roll characteristics are the same for different Reynolds numbers. This result suggests even though the Reynolds number is different between the force measurements and flow visualizations, which will be shown below, it may be possible to make qualitative discussion on the results.

2.2.3 Relationships between the Vortex Breakdown Location and the Static Roll Characteristics

Figure 8 shows the chordwise vortex breakdown position for the inboard vortex formed on the left wing together with C_{roll} versus ϕ at Re=6.2x10^4 for the three models when θ=20° and 26°. These rolling moment data were measured in [12]. This figure shows the estimated chordwise position of the vortex breakdown of the inboard vortex formed on the left wing. The breakdown positions were determined as described in section 2.1. Y-axis on the left side indicates nondimensional position ratios for the distance from the apex to the position of the light sheet, where 0 means the apex and 1 the trailing edge. Please note that C_{roll} is plotted at the roll angles in a range from -10° to 30° to make it easier to see.

Figure 8 shows that the breakdown position of the inboard vortex on the windward wing (left wing, ϕ<0) is relatively insensitive to the roll angle for all the tested cases. On the leeward wing (ϕ>0), the breakdown position rapidly moves from $x/c_r \approx$ 0.75-0.8 to the trailing-edge. This rapid movement of the breakdown position near the trailing-edge was also observed in [7]. This figure also indicates that there is a distinct hysteresis of flow pattern in this rapid movement of breakdown position for some cases (Type B, θ=20° and Type A,

$\theta=26°$). This hysteresis of the flow pattern is seen at the same roll angles where hysteresis in C_{roll} is observed. This result suggests that the inboard vortex strongly affects C_{roll}, and that the hysteresis and abrupt changes in C_{roll} are due to the inboard vortex behaviors.

2.2.4 Interaction between the Inboard and Outboard Vortices

In this section, smoke flow visualization results at $Re=2.9x10^5$ are used to confirm the discussion about the relationships between the static rolling moment and the vortex breakdown discussed in the last section.

Figure 9 shows the visualized pictures at some chordwise locations for three models. Each picture is arranged at a corresponding chordwise position. Outlines of the inboard and outboard vortices formed on the right wing are indicated using dotted lines. A marker "×" shows the center of the inboard vortex estimated by image processing. A marker "+" shows that of the outboard vortex. 30 pictures were captured from the recorded movie for each test case. An average grayscale picture was made from these 30 pictures by image processing. In this picture, positions that are smoke free are black, and positions that are smoke filled are white (Fig. 4). Value of brightness was calculated for each pixel and pixels where the value of brightness is higher than the arbitrarily decided baseline brightness were focused on. The pixels focused on look like a vortex outline circle. The center of vortex was estimated as a center of the circle formed by the vortex outline by using least-squares method. The center of vortex is not indicated when the vortex is completely broken down. These images indicate that only the inboard vortex is formed upstream of the kink, and that both the inboard and outboard vortices are formed downstream of the kink, because of the geometry. The relative position between the inboard and outboard vortices is different among the three models with different outboard sweepback angles. Inboard and outboard vortices on Type A are located relatively far each other, compared to those of Type C.

Figure 10 shows the transition of the inboard vortex core formed on the right wing of the three wing models when the roll angle changes from $\phi=-30°$ to $-10°$ for different chordwise positions at $\theta=20°$. This figure shows that the inboard vortex on the right wing moves inboard as the wing is rolled clockwise direction and that the transitions of the inboard vortex of the three models have a similar tendency.

Figure 11 shows the visualized pictures of the inboard and outboard vortices for three wing models at $x/C_r=0.8$, $\phi=-30°$ and $\theta=20°$. These pictures indicate that distance between the inboard and outboard vortex becomes smaller and the outboard vortex merges with the inboard vortex at the same time, as the inboard vortex pushes it upwards when the outboard sweepback angle becomes larger (from Type A to Type C). It suggests that the interaction between the inboard and outboard vortices becomes stronger when the outboard sweepback angle increases.

Figure 12 shows the results of C_{roll} versus ϕ at the same Reynolds number ($Re=2.9x10^5$) as that of the smoke visualization tests when $\theta=20°$ for the negative roll angle range. In the case of Type A and Type B, roll hysteresis is seen as it was at $Re=8.6x10^5$ shown in Fig. 5. In the case of Type C, distinct hysteresis is not observed near the roll angle $\phi=0°$. However, the hysteresis would be observed more clearly if measurement had been conducted at smaller increments of the roll angle as in Fig. 6.

Figure 13 shows the hysteresis of breakdown position captured in the visualized pictures of inboard and outboard vortices. As mentioned above, the vortex breakdown is an unsteady phenomenon, so it is difficult to measure the position of breakdown accurately. Here, "vortex breakdown ratio" is defined. The thirty pictures captured from the visualization movies were selected randomly. The vortex breakdown ratio is defined as the ratio between the number of pictures where the vortex breaks down is observed and the complete set of all 30 captured pictures. The vortex is considered to be broken down when the core of it looks white, because the flow velocity around the core is low and the core is filled with white smoke when broken down. In the same way, it was considered not to be broken down when the core

of it looks black. Vortex breakdown ratio of 1 means complete breakdown and vortex breakdown ratio of 0 no breakdown. Figure13–a and -b shows the visualized pictures of the vortices on the right wing for Type A at ϕ=-12°, θ=20° and x/C_r=0.8 when the wing is rolled clockwise and counter-clockwise directions. Figure 8 measured at Re=6.2x10^4 indicated the hysteresis of breakdown is observed downstream of x/C_r=0.8. Therefore, the present measurement was made at the same chordwise position of x/C_r=0.8. Numerical values of "vortex breakdown ratio" are indicated on the picture both for the inboard and outboard vortices. Different vortex breakdown ratios are seen both for the inboard and outboard vortices. In the counter-clockwise direction (Fig. 13-a), a higher value is seen than that in the clockwise direction (Fig. 13-b) for the inboard vortex, and adverse results are obtained for the outboard vortex. Figure 5 indicated that at the roll angles where C_{roll} hysteresis is seen, higher rolling moment is observed in the counter-clockwise direction than in the clockwise direction. This suggests that smaller lift acts on the right wing in the counter-clockwise direction than that in the clockwise direction. When the vortex breakdown position moves upstream, the vortex lift acted on the wing becomes smaller. In this case, the result of the inboard vortex breakdown ratio holds true to this discussion, however, the outboard vortex breakdown ratio shows an opposite trend. This suggests that the inboard vortex affects the static roll characteristics more strongly than the outboard vortex. Figure 13–c and -d shows the case with Type C at the roll angle ϕ=-3.5°, and at the chordwise position of x/C_r=0.9. The vortex breakdown ratio is clearly different for the rolling direction. These results agree with the observations discussed in Fig. 8 that was measured at lower Reynolds number.

Oil flow visualization tests for three models were conducted to confirm the observations discussed in Fig. 11 at Re=8.6x10^5, θ=20°, ϕ=0°. Figure 14 shows visualization results of the flow pattern for the three models. The illustration of flow pattern is also shown. Comparing the attachment area (i.e. area where vortex attaches to the wing surface) of the outboard vortex with Type A and Type B, the area on Type B, whose outboard sweepback angle is larger than that of Type A, is smaller than that on Type A. When the outboard vortex gets close to the inboard vortex, it is brought upward. This flow pattern suggests that the vortices on Type B have this tendency more strongly than Type A. There is no attachment area of the outboard vortex with Type C. This suggests that the outboard vortex is merged with the inboard vortex as soon as it separates from the leading edge. These results confirm the discussion in Fig. 11 that the interaction between the inboard and outboard vortices becomes stronger when the outboard sweepback angle becomes larger.

2.2.5 Discussion

The visualization results indicated that the inboard and outboard vortices get closer and the interaction between them increases for the cranked arrow wing as the outboard wing sweepback angle increases. The results of the force measurements of C_{roll} at different Reynolds number indicated that the overall static roll characteristics measured at different Reynolds number do not change qualitatively. These results led to us the conclusion that visualization results can be applied to the discussion for the force measurements although the force measurements and the visualization tests were conducted at different Reynolds numbers.

From the results of the force measurements, the range of the roll angle, where the C_{roll} hysteresis is observed, is narrower for the cranked arrow wing with the more highly sweptback outboard wing.

Reference [7] investigated the effects of outboard leading-edge flap deflection and revealed that the roll characteristics with large hysteresis are observed for the cranked arrow wing with outboard flap deflection, because the inboard and outboard vortices are independently located and are not strongly interacting each other.

All discussion described above indicate that the cranked arrow wing with the highly sweptback outboard wing has a tendency to have static roll characteristics without large hysteresis, and this is due to the closer

interaction between the inboard and outboard vortices.

3 Effects of the Other Planform Parameters

In the previous section, the relationships between the static roll characteristics and the vortex behavior were discussed by the results of three types of models with different outboard sweepback angles. In this section, other planform parameters of the cranked arrow wing are focused on; the sweepback angles of the inboard wing and the spanwise location of the kink. Low speed wind tunnel tests were conducted to investigate the effects of these parameters on the static roll characteristics and the vortex behaviors.

3.1 Experimental Details

Figure 15 shows details of the five flat plate cranked arrow wing models with different inboard sweepback angles and with different spanwise location of the kink. Type 1 is similar to the original models however it is $(1/2)^{0.5}$ scale of the original Type B models. The wing area of all the tested models is $0.206 m^2$ and its thickness is 0.008m. Only the edges of the upper surfaces are beveled. Although all tests were made at a tunnel speed of U_∞=30m/s, Reynolds number based on the mean aerodynamic chord is different for each model because of their different mean aerodynamic chord. The range of Reynolds number is from 5.2×10^5 to 8.5×10^5. The inboard sweepback angles for Type 2 (56°) and Type 3 (76°) differs from that of Type 1 (66°) however they have the same outboard sweepback angle (42°) and the same spanwise location of the kink (b_{kink}/b_{max}=0.55). The spanwise location of the kink for Type 4 (b_{kink}/b_{max}=0.40) and Type 5 (b_{kink}/b_{max}=0.70) differs from that of Type 1. However, they have the same inboard (66°) and outboard sweepback (42°) angles.

The experiments were made in a 2m x 2m circuit type low-speed wind tunnel at the Japan Aerospace Exploration Agency. The incidence angle θ was in a range from 12° to 26°. Rolling moment was measured using a six-component balance. The model was attached to the balance

with a sting and can be rotated around its center axis along with the balance. The rolling moment is the roll component around the model center axis (Fig. 3). The rolling moment coefficient C_{roll} has been obtained by rolling the model at 2.5° increments from ϕ=0° to +30° and by rolling back from ϕ=+30° to 0° which completes one measurement cycle.

Oil flow visualization tests at U_∞=30m/s were also made to describe the surface flow pattern.

3.2 Results and Discussion

3.2.1 Effect of Different Inboard Sweepback Angles

In this section, the effect of different inboard sweepback angles on the static roll characteristics is described comparing the results of Type 1, Type 2 and Type 3.

Figure 16-a shows the results of C_{roll} versus ϕ for different θ with the different inboard sweepback angles. Please note that C_{roll} is plotted only for the positive roll angles. This figure indicates a linear restoring rolling moment until θ=16°. Nonlinear rolling moment characteristics are seen at θ higher than 20° except for Type 2. Abrupt changes and C_{roll} hysteresis are seen from θ=20° to 26° except for Type 2. The difference between the inboard and outboard sweepback angle of Type 2 is 14° and is very small compared to that of other models. In other words, Type 2 model is relatively similar to the planar delta wing. It is thought that this similarity is the reason why abrupt change and C_{roll} changes are not seen for Type 2. Comparing the results of C_{roll} for three model types at the same incidence angle, the range of the roll angle ϕ, where hysteresis is observed, becomes wider when the inboard sweepback angle becomes larger (from Type 2 to Type 3). The range of the roll angle ϕ, where hysteresis is observed for Type 1, is narrower than that estimated from Fig. 7 at θ=20° for Type B. It is thought that this is partly due to the different section shapes of the models. The upper and lower surfaces of all edges of Type B are beveled but only the upper surface of all edges of Type 1 is beveled.

Figure 17–a, -b and -c show results of the oil flow visualizations. Although attachment area of the outboard vortex is seen from the kink to the trailing edge for Type 3, whose inboard sweepback angle is the largest among three models, no attachment is observed downstream of the yellow area in the picture for Type 1. For Type 2, there is no attachment of the outboard vortex. This suggests that the outboard vortex is merged with the inboard vortex for the model with the small inboard sweepback angles, because the distance between the inboard and outboard vortices is small.

3.2.2 Effect of Different Kink Locations

In this section, the effect of different kink locations on the static roll characteristics is described comparing the results of Type 1, Type 4 and Type 5.

Figure 16-b shows the results with the different spanwise location of the kink. This figure indicates a linear restoring rolling moment until $\theta=16°$. Nonlinear rolling moment characteristics are observed at θ higher than 20°. Abrupt changes and C_{roll} hysteresis are seen at $\theta=20°$ to 26°. The range of the roll angle ϕ, where hysteresis is observed, is very wide for Type 4 compared to Type 1 and Type 5. The reason for this is assumed to be because of the different magnitudes of the inboard vortex downstream the kink for Type 4 and the other two models. For the model which has the kink far from the center axis (i.e. Type 5), the chordwise relative distance from the apex to the kink to C_r is long. The inboard vortex grows well on that model. It is assumed that the difference of the range of the roll angle ϕ, where hysteresis is observed, for Type 4, Type 1 and Type 5 is derived from the difference between the relative magnitudes of the inboard and outboard vortices for the models.

Figure 17–a, -d and -e shows oil flow visualization results. Attachment area of the outboard vortex is seen from the kink to the trailing edge for Type 5, whose kink is located nearest to the wing tip among the three models. The outboard vortex for Type 1 is merged with the inboard vortex downstream of the attachment area. For Type 4, whose kink is located nearer to the wing root than the kink for

Type 1, the location of the attachment area is more upstream than that of Type 1. These results indicate that the distance between the inboard and outboard vortices for the models with different spanwise location of the kink is not largely different, but the merge characteristics of the inboard and outboard vortices on the three models with different spanwise kink location are clearly different.

3.2.3 Discussion

The results of the force measurements indicated that the range of the roll angle ϕ, where hysteresis is observed, becomes wider when the inboard sweepback angle becomes larger. From the results of visualization tests, it is thought that the interaction between the inboard and outboard vortices is small for the cranked arrow wing with highly sweptback inboard wing. For the cranked arrow wing with highly sweptback inboard wing, the interaction between the inboard and outboard vortices is small and hysteresis is widely observed. This confirms the discussion described in section 2.2 about the effects of the interaction on the C_{roll} hysteresis. Furthermore, with the discussion about the effects of the outboard sweepback angle, when the difference between the inboard and outboard sweepback angles is small, in other words, cranked arrow wing is similar to the planar delta wing, the interaction between the inboard and outboard vortices is strong and the static rolling moment hysteresis tends to be observed only in a narrow roll angle range.

In summary, the present results indicated that the relative magnitude and location between the inboard and outboard vortices control the interaction and merge between these vortices. Vortex breakdown and hysteresis characteristics of static rolling moment are mainly affected by them.

4. Conclusions

Wind tunnel measurements were done on a cranked arrow wing configuration with different wing planforms. The purpose of the measurements is to discuss the effect of different parameters of cranked arrow wing

planforms on the static roll characteristics and the interaction between the inboard and outboard vortices. Three parameters were focused here: outboard wing sweepback angles, inboard wing sweepback angles, and inboard / outboard wing kink locations.

1) The inboard vortex behaviors are strongly influenced by the differences of outboard wing sweepback angles and thus the different rolling moment characteristics such as a hysteresis and abrupt changes in the rolling moment were observed.

2) At different Reynolds numbers, values of the static rolling moments are different; however the relative roll characteristics do not change.

3) It was confirmed from the flow visualization analysis that the rolling moment hysteresis is caused by the different chordwise position of inboard vortex breakdown when the wing is rotated in the clockwise and counter-clockwise directions.

4) The wing with the less-highly sweptback outboard wing has a tendency to have static roll characteristics with large hysteresis, and this is due to the weaker interaction between the inboard and outboard vortices.

5) When the difference between the inboard and outboard sweepback angles is small, in other words, cranked arrow wing is similar to the planar delta wing, the interaction between the inboard and outboard vortices is strong and the static rolling moment hysteresis tends to be observed only in a narrow roll angle range.

6) Interaction and merge between the inboard and outboard vortices depend on the relative magnitudes of them, which affects hysteresis characteristics for the static rolling moment and vortex breakdown.

References

[1] Yoshida K and Makino Y. Aerodynamic Design of Unmanned and Scaled Supersonic Experimental Airplane in Japan, Finland, ECCOMAS 2004.

[2] Brennenstuhl U and Hummel D. Vortex Formation over Double-Delta Wings, Proceedings of 13th Congress of the International Council of the Aeronautical Sciences (ICAS Paper 82-6.6.3), Seattle, USA, Aug. 1982, pp.1302-1309.

[3] Orsen P E and Nelson R C. Vortex Interaction Over Double Delta Wings at High Angles of Attack, AIAA Paper 89-2191, Jul. 1989.

[4] Erickson G E. The Fluid Mechanics of Slender Wing Rock, *Journal of Aircraft*, Vol.21, No.5, pp 322-328, 1984.

[5] Hanff E S and Jenkins S B. Large-Amplitude High-Rate Roll Experiments on a Delta and Double Delta Wing, AIAA Paper 90-0224, Jan. 1990.

[6] Kwak D Y, Noguchi M, Shirotake M and Rinoie K. Rolling Moment Characteristics of Supersonic Transport Configuration at High Incidence Angles, *Journal of Aircraft*, Vol.43, No.4, pp 1112-1119, 2006.

[7] Rinoie K, Shirotake M and Kwak D Y. Vortex Behaviors of Rolled Supersonic Transport Configuration with Leading-Edge Vortex Flaps, *Journal of Aircraft*, Vol.43, No.6, pp 1904-1913, 2006.

[8] Verhaagen N G, Jenkins L N, Kern S B and Washburn A. E. A Study of the Vortex Flow over a 76/40-deg Double-Delta Wing, AIAA Paper 95-0650, Jan. 1995.

[9] Gursul I and Yang H. On Fluctuations of Vortex Breakdown Location, *Physics of Fluids*, Vol.7, No.1, pp 229-231, 1995.

[10] Jobe C E, Hsia A H, Jenkins J E and Addington A. Critical States and Flow Structure on a 65-Ddeg Delta Wing, *Journal of Aircraft*, Vol.33, No.2, pp 347-352, 1996.

[11] Katz J and Levin D. Static Measurements of Slender Delta Wing Rolling Moment Hysteresis, *Journal of Aircraft*, Vol.28, No.4, pp 282-283, 1991

[12] Rinoie K, Imai G, Shirotake M, Sunada Y and Kwak D Y, Roll Characteristics of SST Configuration with Different Outboard Wing Sweepback Angles (in Japanese), Proc. 36th Annual Conference of the Japan Society for Aeronautical and Space Sciences, 1B1, Tokyo, Apr. 2005, pp.69-72.
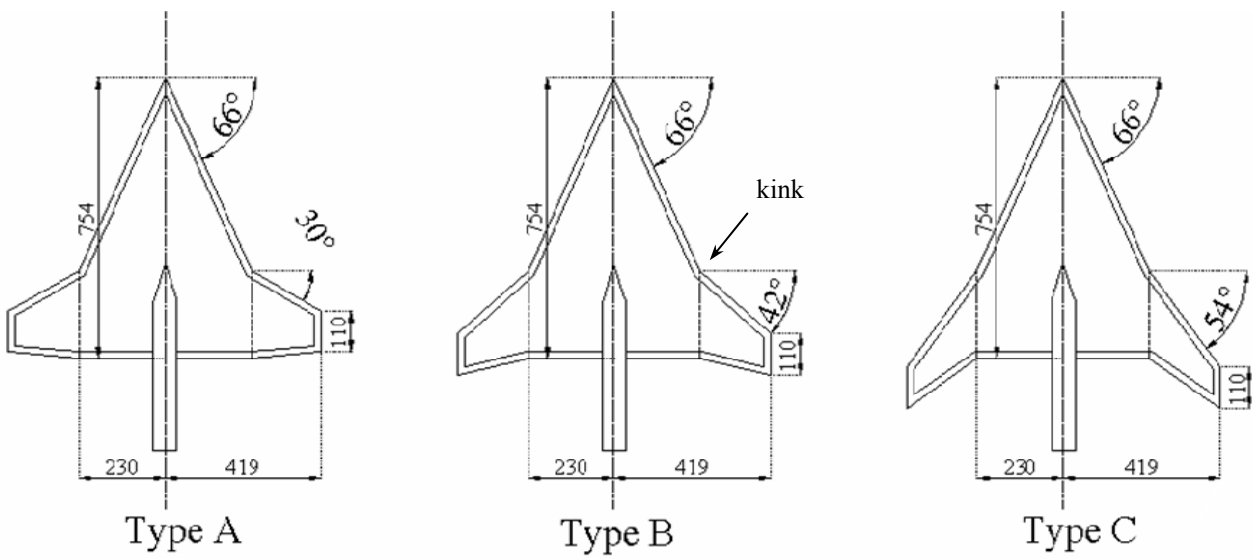
Copyright Statement

Fig.1   Three type cranked arrow flat plate models

with different outboard sweepback angles, in millimeters

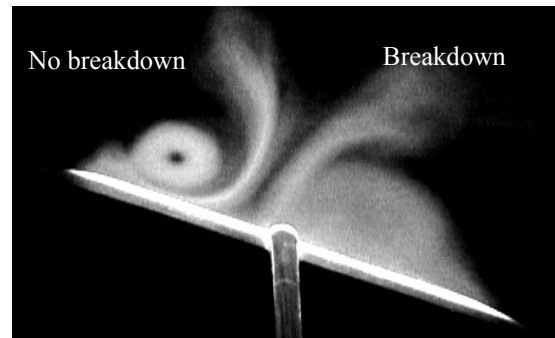Fig.2   2m x 2m circuit type low-speed wind tunnel

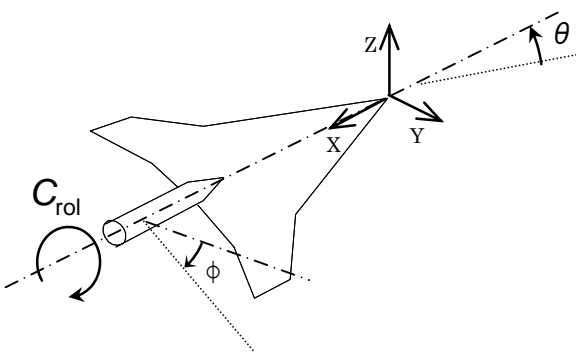Fig.4   Visualized inboard vortex on the left wing

Fig.3   x-, y- and z- coordinate

Type A
($\Lambda_{in/out}$=66°/30°)

Type B
($\Lambda_{in/out}$=66°/42°)

Type C
($\Lambda_{in/out}$=66°/54°)

Incidence angle θ

C_{rol} [1unit:0.05]

30°
28°
26°
24°
22°
20°
18°
16°
12°

Counter-Clockwise

Clockwise

-30°-20°-10° 0° 10° 20° 30°   -30°-20°-10° 0° 10° 20° 30°   -30°-20°-10° 0° 10° 20° 30°

Roll angle ϕ [deg]
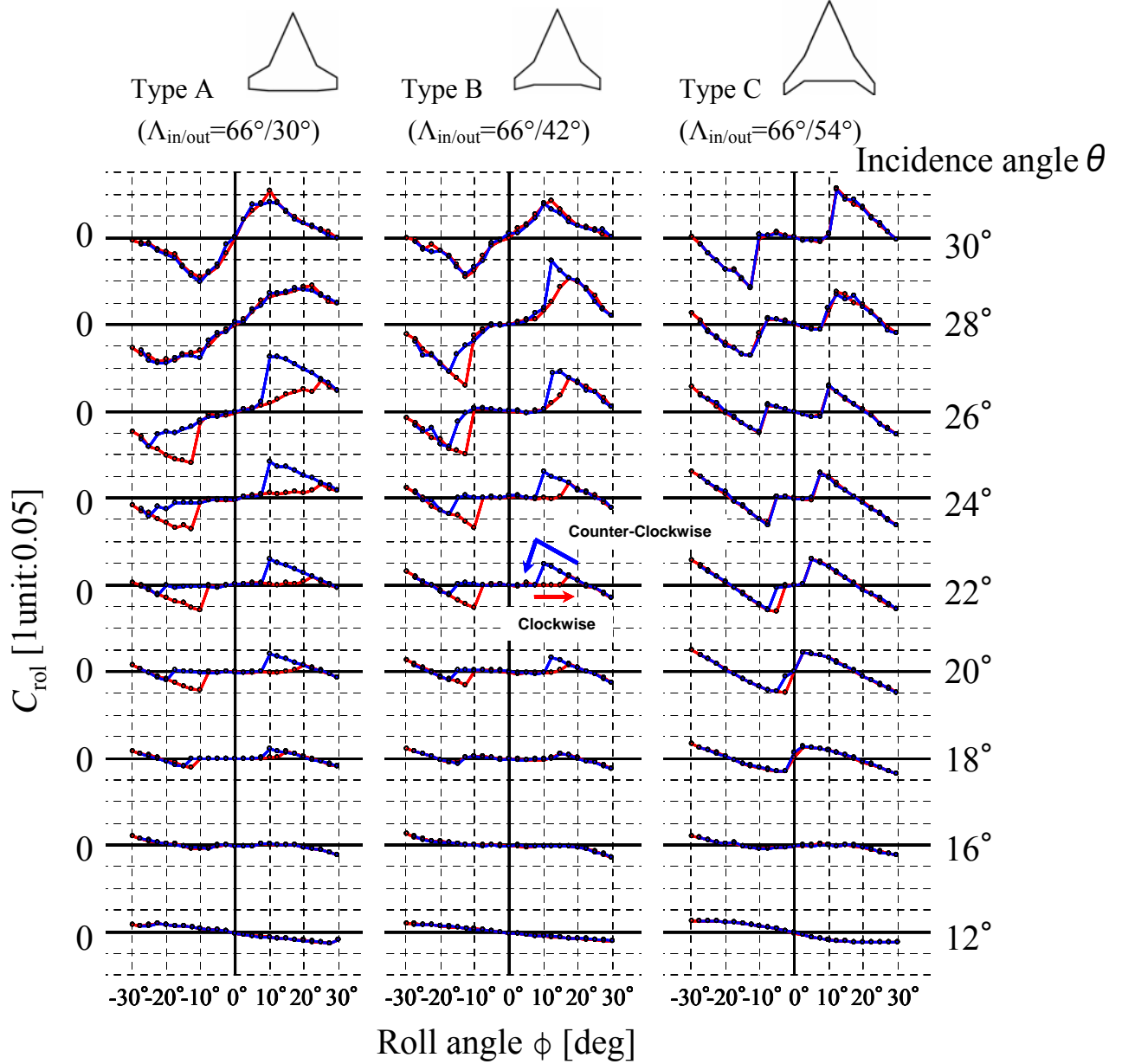
Fig.5   Rolling moment characteristics at different incidence angles (Re=8.6×10⁵)

0.015

C_{rol}

0

-0.015

-8   -6   -4   -2   0   2   4   6   8

ϕ [deg]
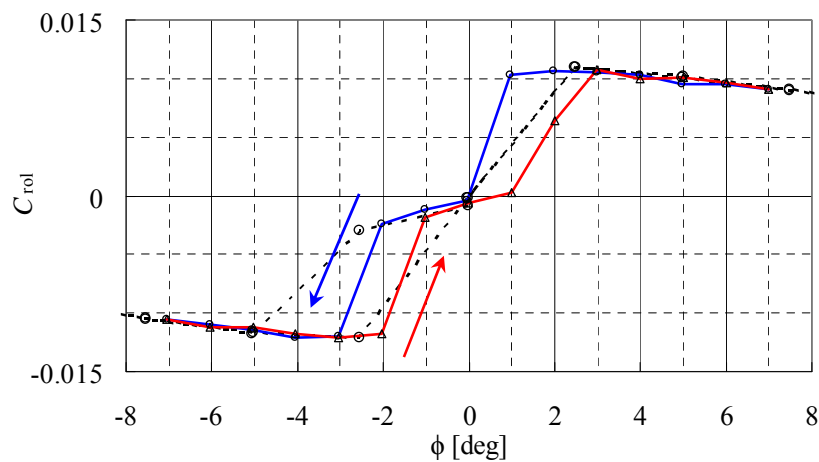
Fig.6   Rolling moment characteristics obtained by the detailed measurement (Type C, θ=20°)

(Dotted lines: results from Fig.5.)
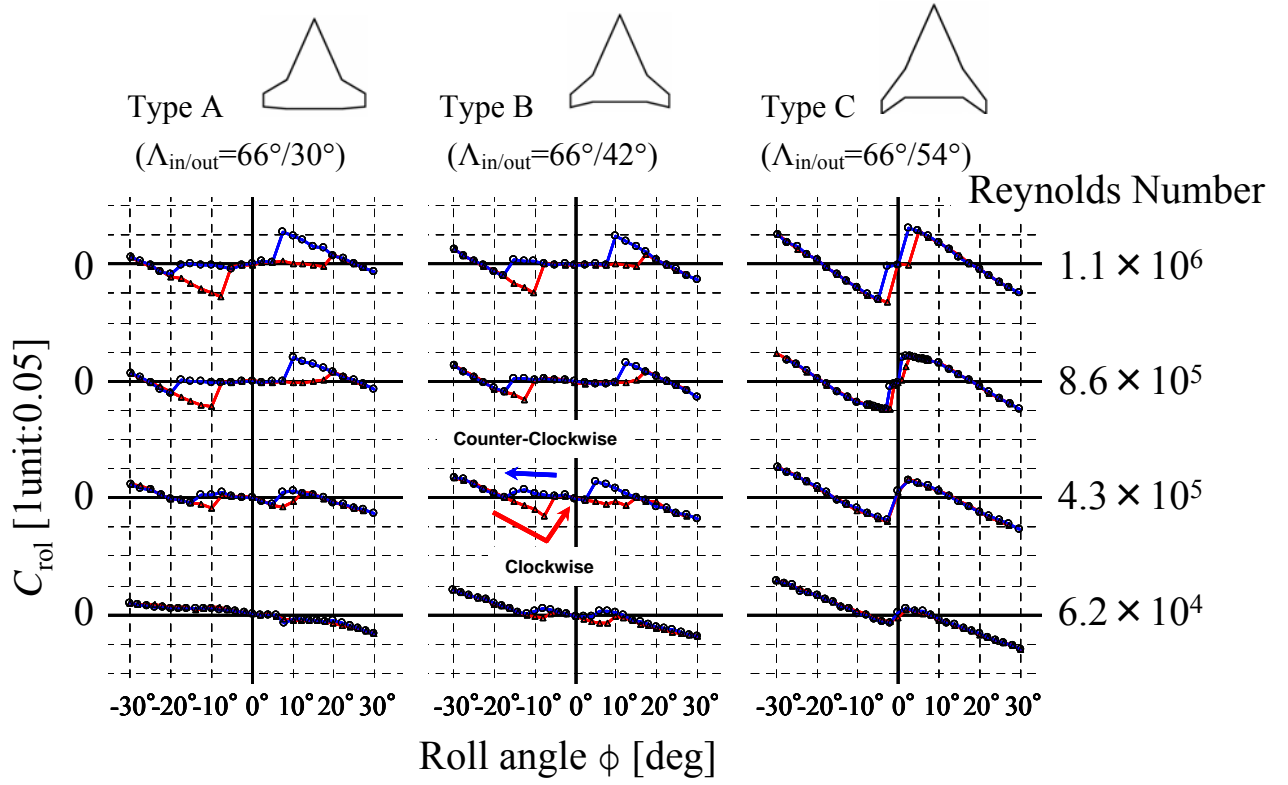
Fig.7   Rolling moment characteristics at different Reynolds numbers

a) Type A (Λ_{out}=30°), θ=20°

b) Type A (Λ_{out}=30°), θ=26°

c) Type B (Λ_{out}=42°), θ=20°

d) Type B (Λ_{out}=42°), θ=26°

e) Type C (Λ_{out}=54°), θ=20°

f) Type C (Λ_{out}=54°), θ=26°
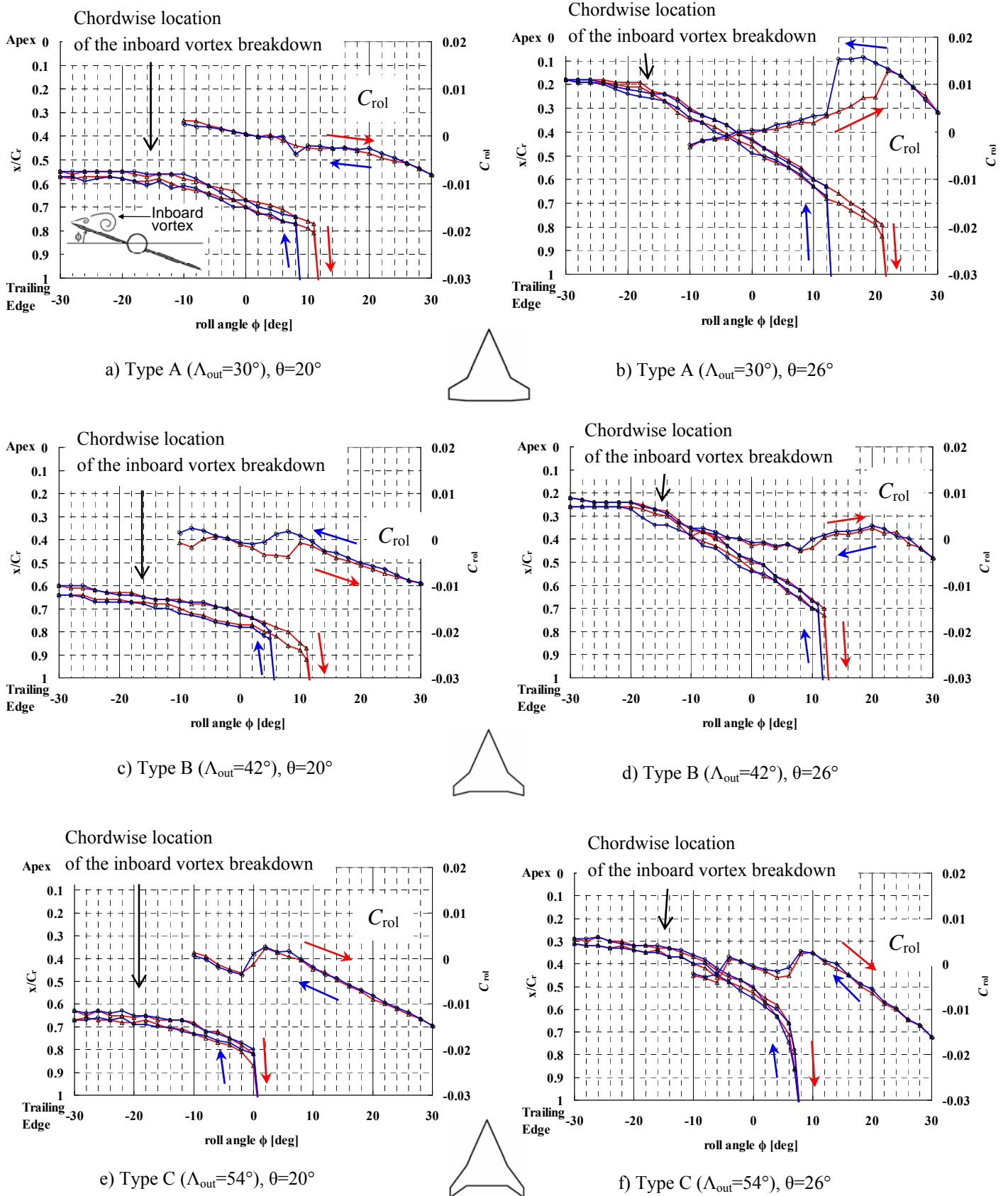
Fig.8   Chordwise location of the vortex breakdown on the left inboard wing and the roll characteristics (Re=6.2×10^4)

a) Type A (Λ_{out}=30°) b) Type B (Λ_{out}=42°) c) Type C (Λ_{out}=54°)
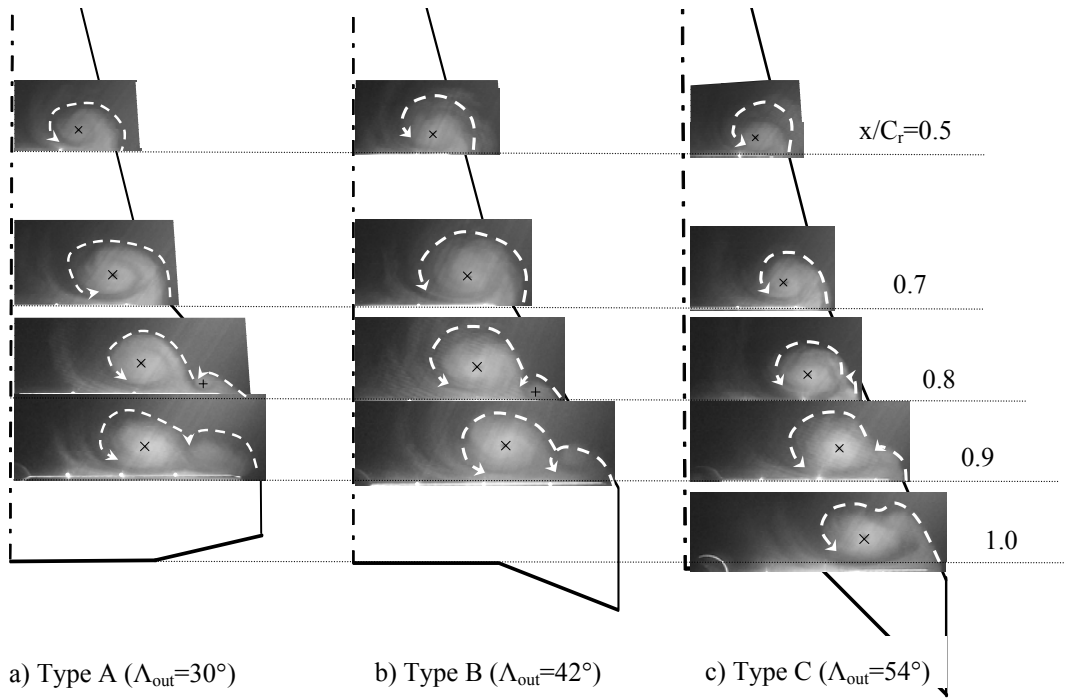
Fig.9   Visualized inboard and outboard vortices on the right wing (Re=2.9×10⁵, θ = 20°, ϕ =-30°)
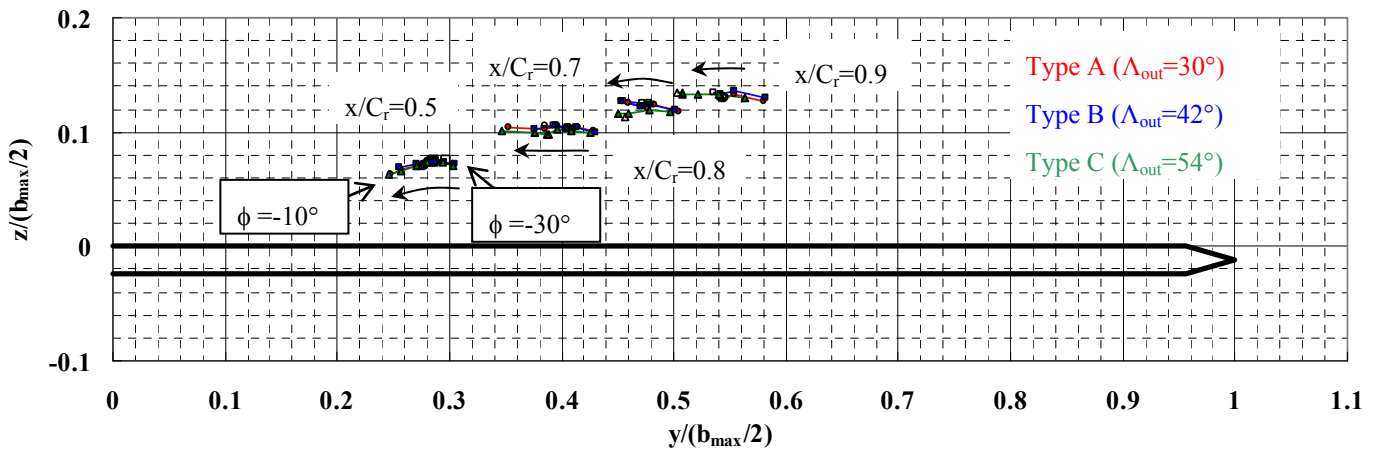
Fig.10   Positions of the inboard vortex core when the model rolls (Re=2.9×10⁵, θ = 20°)

a) Type A (Λ_{out}=30°) b) Type B (Λ_{out}=42°) c) Type C (Λ_{out}=54°)
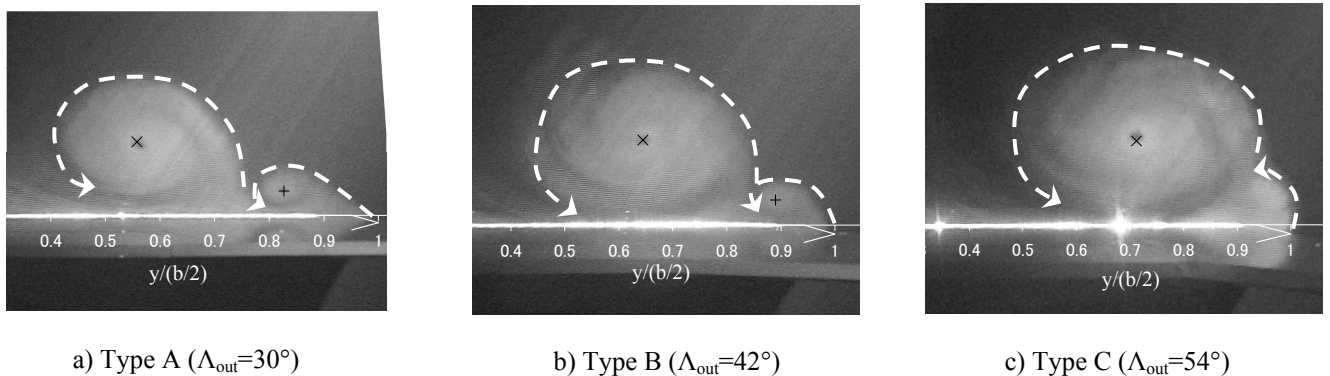
Fig.11   Outline of the inboard and the outboard vortices (Re=2.9×10⁵, θ = 20°, ϕ=-30°, x/C_r=0.8)

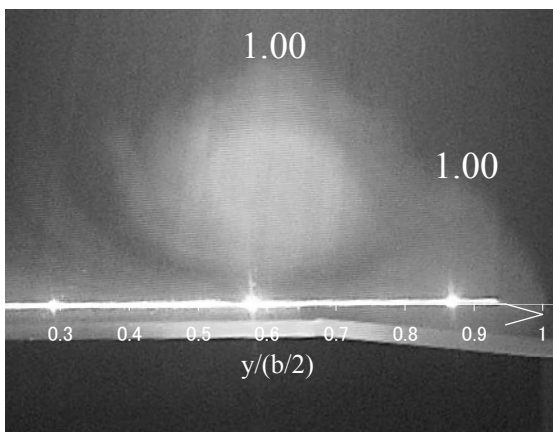a) Type A (Λ_{out}=30°)   b) Type B (Λ_{out}=42°)   c) Type C (Λ_{out}=54°)
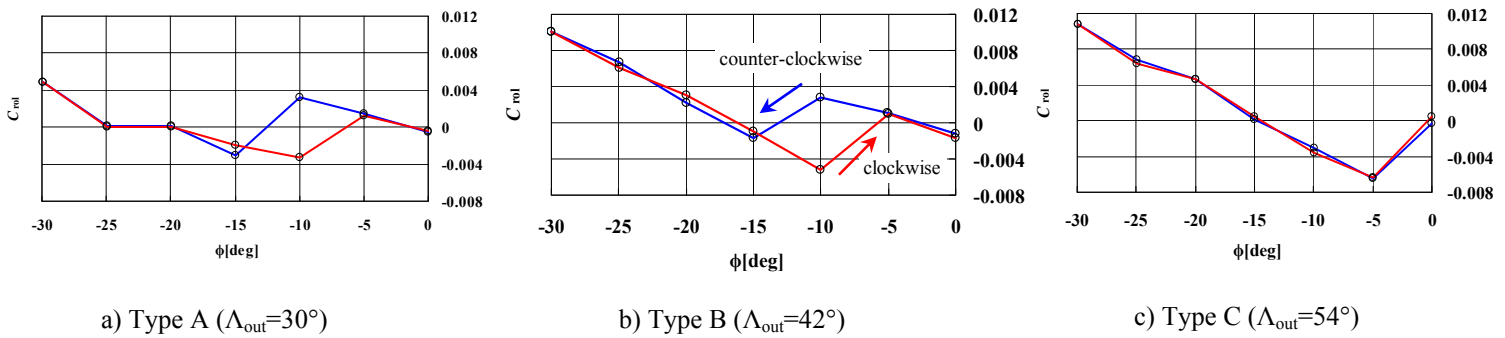
Fig.12   Rolling moment characteristics at the same Reynolds number, where visualization studies were conducted (Re=2.9×10^5, θ = 20°)
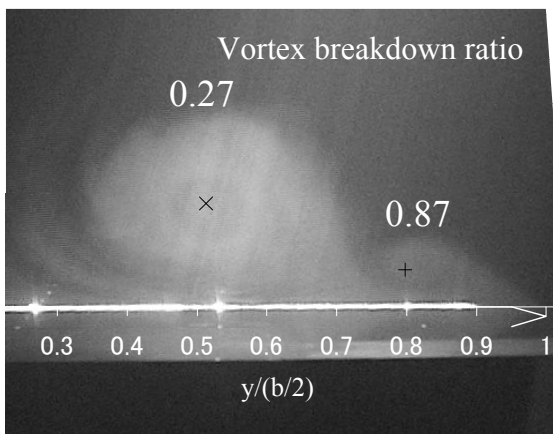
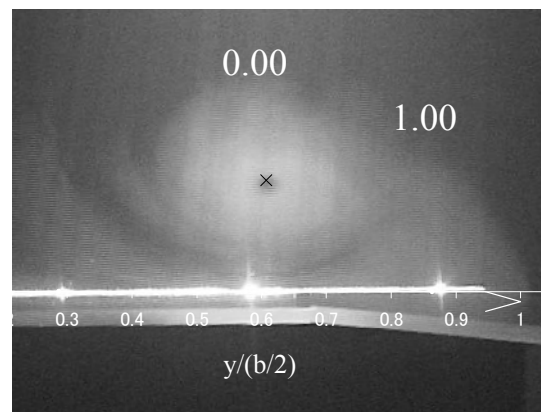a) Type A (Λ_{out}=30°), ϕ=-12°, x/C_r=0.8, counter-clockwise
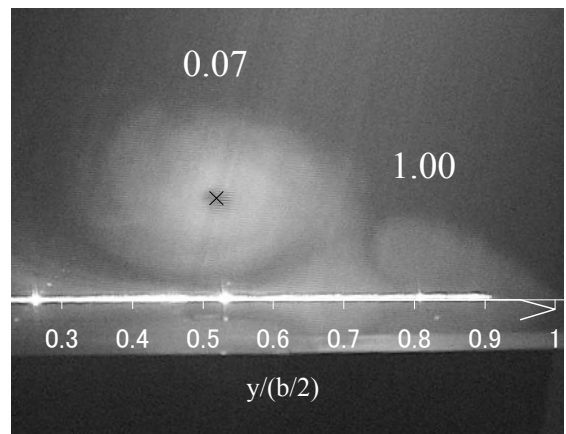
b) Type A (Λ_{out}=30°), ϕ=-12°, x/C_r=0.8, clockwise

c) Type C (Λ_{out}=54°), ϕ=-3.5°, x/C_r=0.9, counter-clockwise

d) Type C (Λ_{out}=54°), ϕ=-3.5°, x/C_r=0.9, clockwise

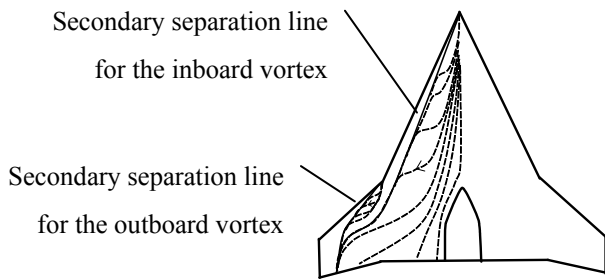Fig.13   Vortex breakdown ratio for the right wing (Re=2.9×10^5, θ = 20°)

Secondary separation line
for the inboard vortex

Secondary separation line
for the outboard vortex

Illustration of flow pattern on the cranked arrow wing

Attachment area
of the outboard vortex

a) Type A (Λ_{out}=30°)   b) Type B (Λ_{out}=42°)   c) Type C (Λ_{out}=54°)
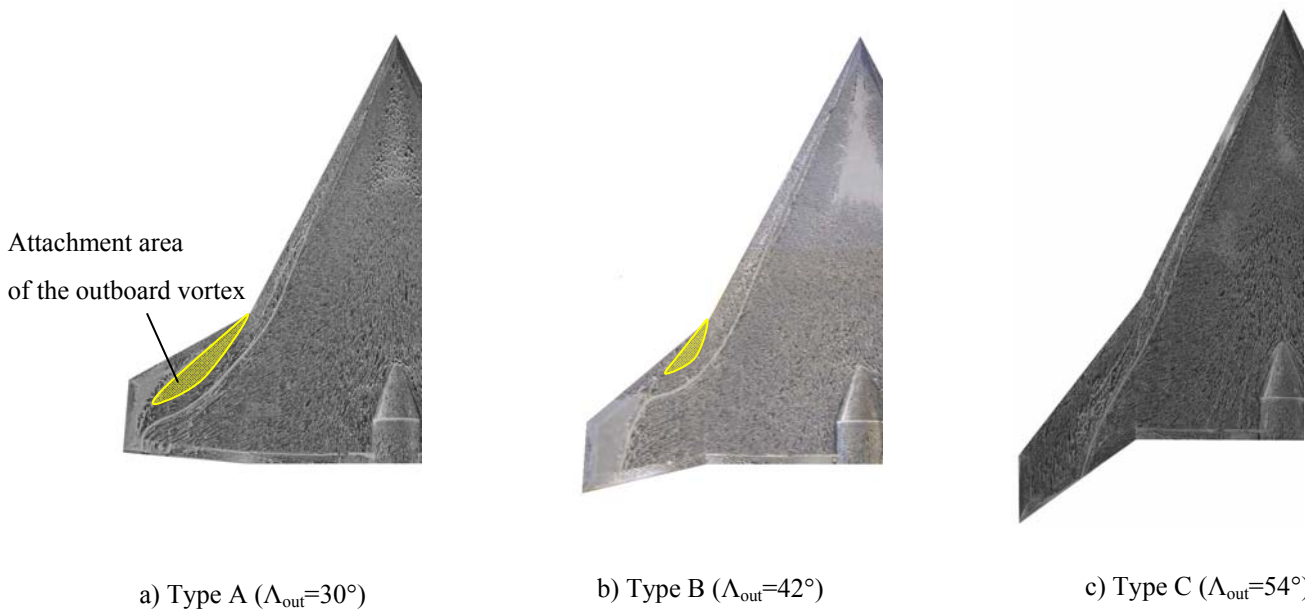
Fig.14   Flow pattern obtained by oil-flow visualization (Re=8.6×10^5, θ = 20°, φ=0°)

Λ_{in}

Λ_{out}

b_{kink}

b_{max}

a) Type 1   b) Type 2   c) Type 3   d) Type 4   e) Type 5
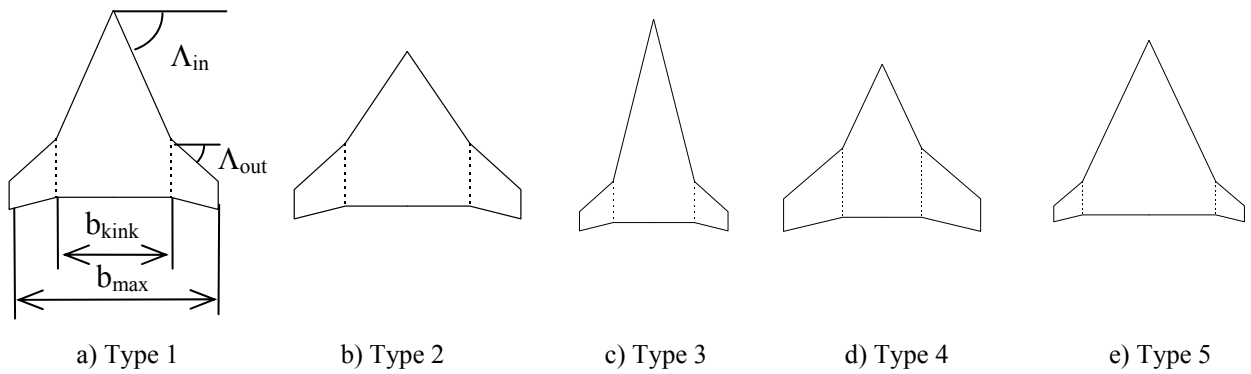
	Type1	Type2	Type3	Type4	Type5
Aspect ratio	2.39	2.80	1.84	2.50	2.24
Mean aerodynamic chord	325mm	277mm	426mm	292mm	355mm
Re	6.1×10^5	5.2×10^6	8.0×10^5	5.5×10^5	6.7×10^5
Λ_{in}	66°	56°	76°	66°	66°
Λ_{out}	42°	42°	42°	42°	42°
Chordwise location of the kink b_{kink}/b_{max}	0.55	0.55	0.55	0.4	0.7

Fig.15   Five type cranked arrow flat plate models

with different inboard sweepback angles (Type 2 and Type 3)

and with different spanwise location of the kink (Type 4 and Type 5)

a) Effect of the inboard sweepback angle

b) Effect of the spanwise location of the kink

Fig.16   Rolling moment characteristics at different incidence angles

Attachment area
of the outboard vortex

a) Type 1 (Λ_{in}=66°, b_{kink} /b_{max}=0.55)

b) Type 2 (Λ_{in}=56°)

c) Type 3 (Λ_{in}=76°)

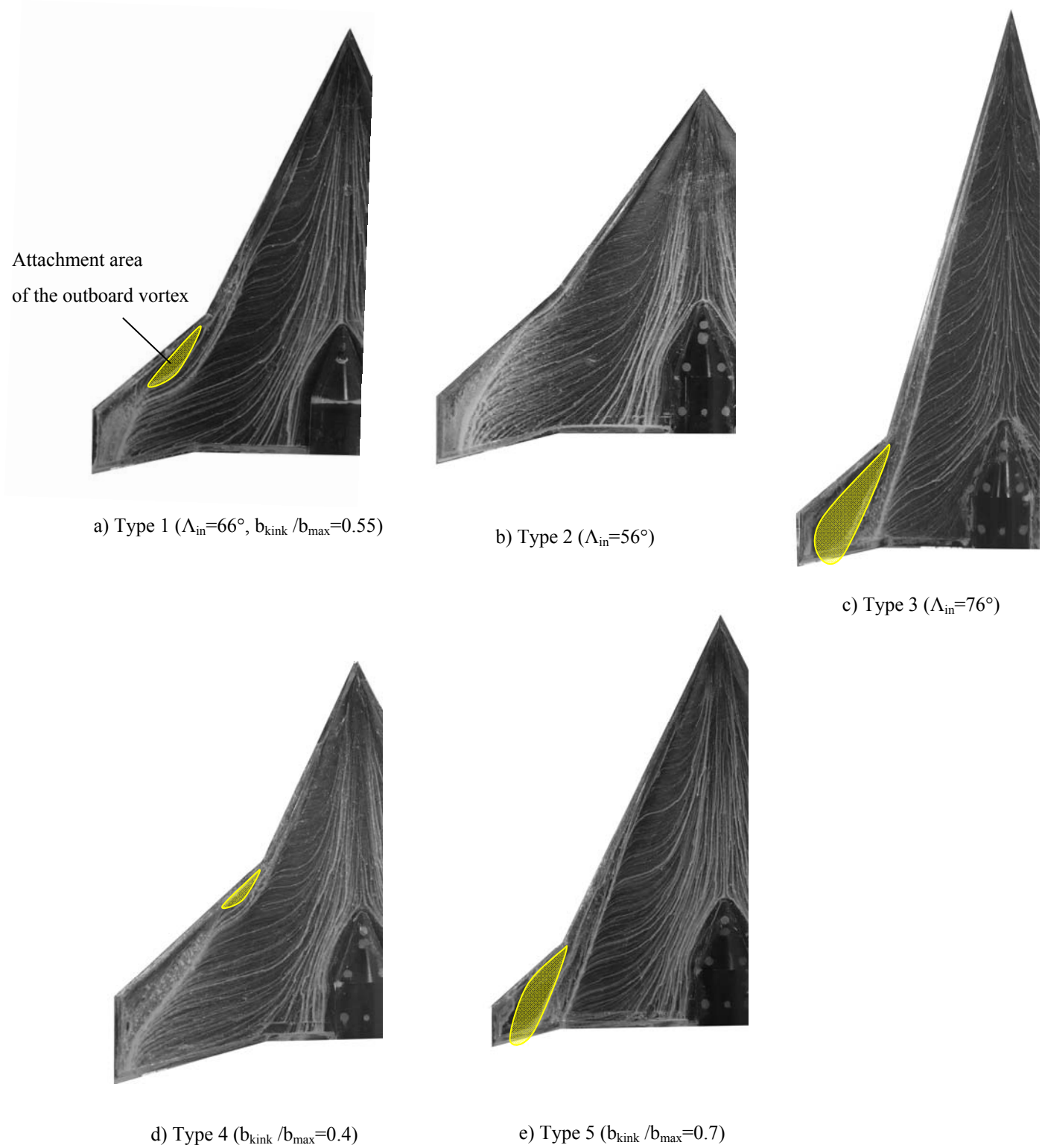d) Type 4 (b_{kink} /b_{max}=0.4)

e) Type 5 (b_{kink} /b_{max}=0.7)
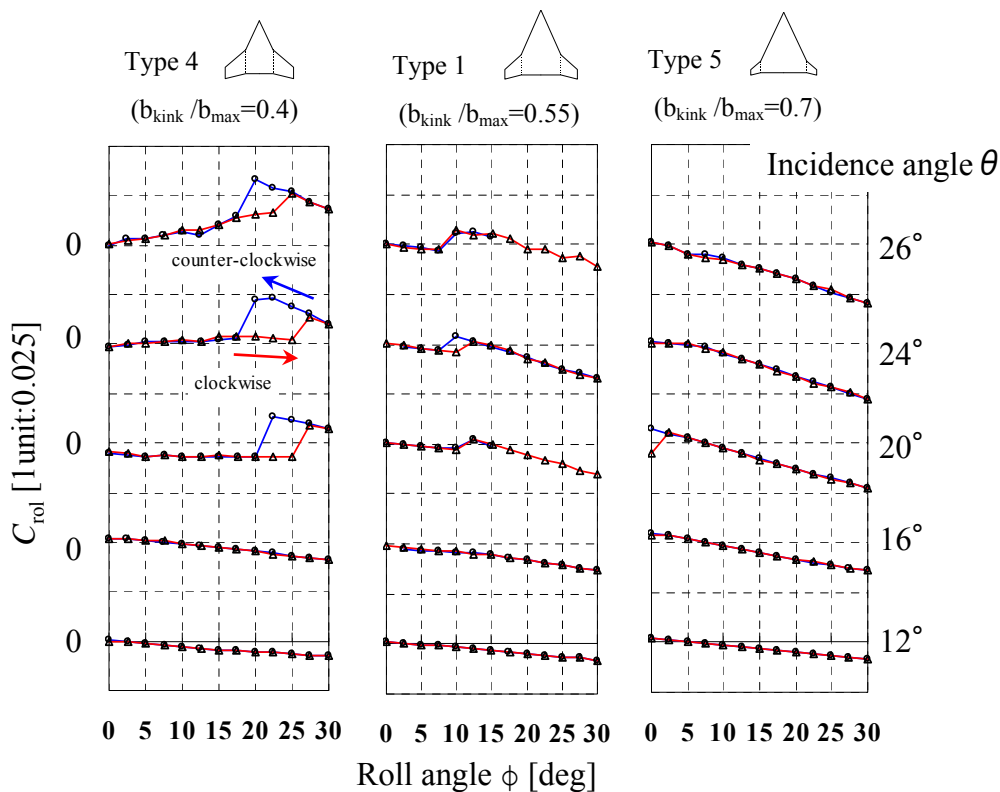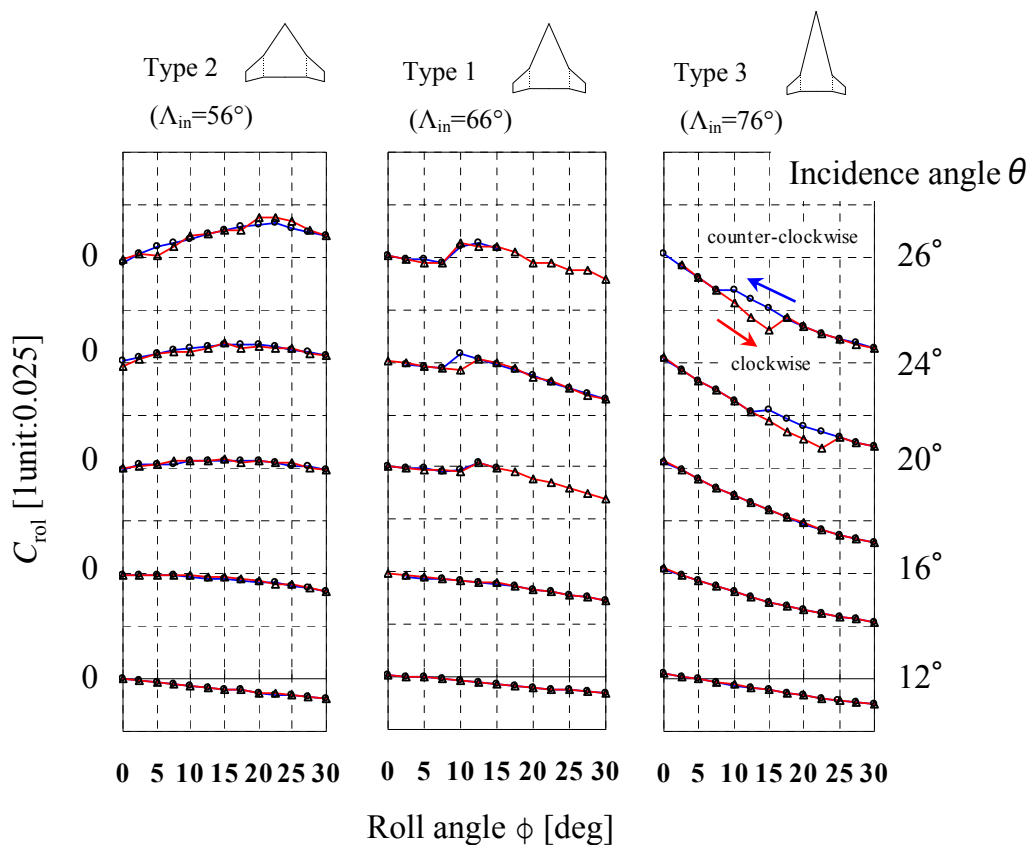
Fig.17   Flow pattern obtained by oil-flow visualization (U_∞=30m/s, $\theta = 20°$, ϕ=0°)